RANS representation of transition and separation over a low-Re number blade section at high angle of attack

Journal of Physics: Conference Series **2766** (2024) 012086 doi:10.1088/1742-6596/2766/1/012086

RANS representation of transition and separation over a low-Re number blade section at high angle of attack

L Pagliarini[1], R Corsini[2], E Stalio[2] and F Bozzoli[1]

[1]Department of Engineering and Architecture, University of Parma, Parco Area delle Scienze 181/A, I-43124 Parma, Italy
[2]Università degli Studi di Modena e Reggio Emilia, Dipartimento di Ingegneria "Enzo Ferrari" via Vivarelli, 10 41125 Modena, Italy

E-mail: luca.pagliarini@unipr.it

Abstract. Systems based on wind energy harvesting can successfully meet part of the increasing green energy demand worldwide. However, wind turbines operation might be undermined by varying atmospheric conditions, which could result in an increase of angle of attack and consequent onset of flow separation phenomena, especially at low Reynolds numbers. Such conditions are strongly influenced by blades geometry, and they negatively affect structural integrity and power output of wind turbines. For this reason, it is crucial to define a tool capable of swiftly allowing numerical investigations on different geometrical configurations to delay and mitigate flow separation occurrence. The present work aims at modelling laminar-turbulent transition and turbulent flow separation over a wind turbine blade section operating at angle of attack = 15°, Re = 66000 and Pr = 0.71 by means of a steady RANS approach. Turbulence is treated by means of the Transition SST k-ω and the Transition k-kL-ω models. The main aerodynamic and thermal coefficients are evaluated and compared against a high-order accurate DNS database for validation. The results highlight, for the present test case, a better capability of the Transition SST k-ω of perceiving the main thermo-fluid dynamic features of the separated flow over the blade section.

1. Introduction

Renewable energy sources are crucial to mitigate climate change. Wind energy harvesting is expected to become prevalent [1], although large-scale wind farms might have a potential climatic impact. Decentralized installation of small-scale wind turbines can overcome this issue [2]. In these devices, small geometric scale rotors are required to operate within a nominal range of wind speeds and Angles of Attack (AoAs) at low Reynolds numbers ($1x10^4 < Re < 3x10^5$) [3]. A typical feature of low Reynolds number regimes is the formation of a Laminar Separation Bubble (LSB) on the low-pressure surface of the wind turbine blades [4]. In this case, laminar flow experiences a strong adverse pressure gradient on the suction surface with the increase of the angle of attack and separates before transition to turbulence. The separated flow quickly undergoes transition and then reattaches as a turbulent boundary layer on the blade surface, leading to the formation of a short separation bubble. By further increasing the angle of attack, such bubble suddenly bursts, causing an abrupt change of the flow pattern and a significative loss of lift [5]. Due to recent growth of available computational power, passive methods for flow separation control have been focused on numerical optimization of aerofoil design to maximize lift whereas minimizing drag and achieving separation delay at increasing AoAs. However, geometrical

optimization usually deals with either high Reynolds number flows or low AoAs, hence far from flow separation conditions [6,7]. In fact, as stressed by Li et al. [8], geometrical optimization techniques usually fail in regions where flow separation occurs due to wrong parametrization or general non-convergence of the solver. For this reason, design methods found in the literature for wind turbines operating at low Reynolds numbers, i.e., small scale wind turbines, are flawed. Additionally, for the sake of a reliable shape optimization, a priori identification of a turbulence model able to correctly reproduce the process of transition to turbulence should be also addressed [9]. The present preliminary study thus proposes to identify a reliable turbulence model to be used in the shape optimization of a blade profile working in the low Reynolds number regime and with high AoA. To this aim, the separated flow over a NACA 4412 profile is numerically investigated by means of two-dimensional steady Reynolds-Averaged Navier-Stokes (RANS) simulations, based on two different turbulence models, namely the Transition SST k-ω and the Transition k-k_L-ω models. The choice of these RANS transitional models has been driven by promising outcomes provided by previous numerical works investigating similar flow separation conditions [10,11]. Energy equation has been also included to account for heat transfer aspects which may be crucial when dealing with development of effective de-icing solutions [12]. The Reynolds number considered in the present work, based on the chord length and the free-stream velocity, is Re = 66000, the Prandtl number is Pr = 0.71, the angle of attack is AoA = 15°, and the turbulence intensity of the free-stream flow is 5%. Thermo-dynamic quantities provided by the steady RANS simulations are compared with those obtained through a Direct Numerical Simulation (DNS) and with previous experimental investigations.

2. Computational methods

2.1. Mesh and boundary conditions

In the present study, a C-grid was adopted among other possible domain topologies (figure 1). A two-dimensional computational domain was realized by considering the following geometrical extensions, being "c" the blade section chord: 10c along both the upstream and normal directions; 15c along the downstream direction; blade section inclined of 15° with respect to the streamwise direction (corresponding to AoA = 15°). A circular refinement region, with radius equal to 2.5c and centred at 0.5c from the leading edge, was also generated to increase the spatial resolution in separated flow regions. Uniform velocity inlet and zero-gauge pressure outlet conditions were given at the left and right boundaries, respectively, according to the sketch of figure 1. Symmetry conditions were set at top and bottom boundaries. No-slip conditions were imposed at the blade section surface. With regards to boundary conditions for temperature, fixed temperature values of T_0 and T_w, with $T_0 > T_w$, were imposed at the inlet and at the blade section surface, respectively (0: free-stream, w: blade section wall). Concerning the meshing strategy, a hybrid mesh was used for the present investigation (figure 1). The mesh was generated by means of Ansys© Design Modeler (v. 2023 R1). The first layer thickness was imposed such that the requirement y+ < 1 was achieved on the overall blade section surface (growth rate equal to 1.05), over which mesh elements were equally distributed.

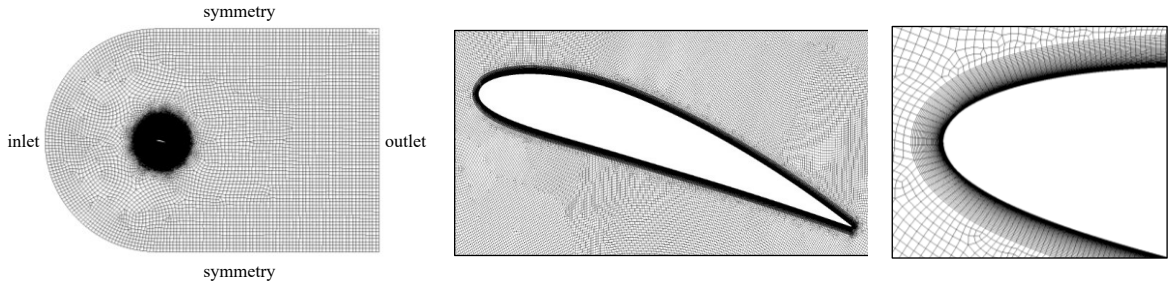

Figure 1: Employed meshing strategy and boundary conditions.

2.2. Numerical procedure

A two-dimensional steady RANS analysis was carried out by adopting two different turbulence models, the Transition SST k-ω [13] with production limiter [14] and the Transition k-k_L-ω [15] models. RANS

equations are derived by averaging incompressible continuity (equation 1) and momentum (equation 2) equations:

$$\frac{\partial U_i}{\partial x_i}=0 \tag{1}$$

$$\frac{\partial U_i}{\partial t}+\frac{\partial\left(U_i U_j\right)}{\partial x_j}=\frac{-1}{\rho}\frac{\partial P}{\partial x_i}+\frac{\partial}{\partial x_j}\left[\nu\left(\frac{\partial U_i}{\partial x_j}+\frac{\partial U_j}{\partial x_i}\right)+\tau_{ij}\right] \tag{2}$$

where U is the averaged velocity in the streamwise and crossflow directions, P is the averaged pressure, ν is the kinematic viscosity, ρ is the density and τ_{ij} is the Reynolds stress tensor. The energy equation is additionally included:

$$\frac{\partial}{\partial t}(T)+\frac{\partial}{\partial x_i}(U_i T)=\frac{\partial}{\partial x_i}\left(\alpha\frac{\partial T}{\partial x_i}\right) \tag{3}$$

being T the temperature and α the air thermal diffusivity. Steady RANS and energy equations are solved numerically through the CFD code Ansys Fluent® (v. 2023 R1), based on the second-order accurate finite volume method. The absolute convergence criterion was set, for all residuals, to 1e-6. A chord-based Reynolds equal to 66000 was considered. The free-stream turbulent kinetic energy was set to obtain a Turbulence Intensity (TI) at the leading edge equal to 5%. Prandtl number equal to 0.71 was used, since it is a representative value for air.

2.3. The reference DNS

The reference DNS was carried out with the well-known open-source code Nek5000 [16]. The continuity equation and the three-dimensional Navier-Stokes equations for incompressible flows were solved numerically based on a high-order spectral element method for spatial discretization. For the present computation spectral elements of order $N = 7$ were used. The time integration is based on a third-order accurate, implicit-explicit scheme. The non-dimensional time step was kept fixed at $\Delta t = 2.5\text{x}10^{-5}$ during the simulation to fulfil a condition $CFL < 0.5$ in each point of the domain. A three-dimensional C-type computational domain was employed. The domain extends 3c upstream of the wing section, 5c downstream, and 0.6c along the spanwise direction. Inflow condition was imposed at the left and top boundaries to obtain a free-stream flow with angle of attack α=15° and fixed temperature T_0. Outflow condition was imposed at the right and bottom boundaries. No-slip and fixed temperature T_w conditions were enforced at the solid walls for velocity and temperature, respectively. Finally, periodicity was used in the spanwise direction. Synthetic inflow turbulence is generated on a plane located 1c upstream of the leading edge of the blade to obtain a free-stream turbulence intensity of TI=5%. The number of elements was $N_E = 2'886'400$, which corresponds to almost 1 billion of degrees of freedom. In the near-wall region the spatial resolution meets the following characteristics $\Delta x^+ \leq 10$, $\Delta y^+ \leq 0.45$, and $\Delta z^+ \leq 7.5$.

3. Results

3.1. Grid independence

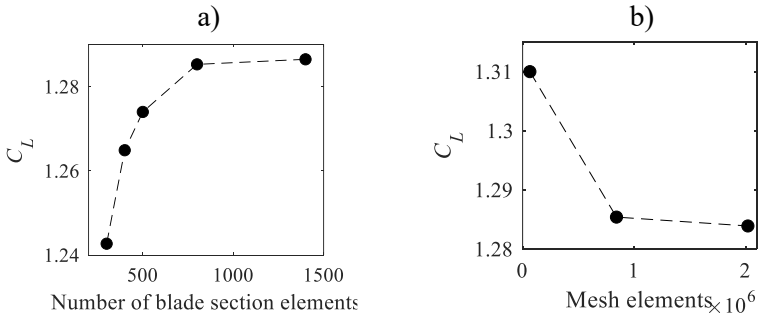

Figure 2: Lift coefficient against elements around the blade section (a) and overall elements (b).

The computational grids considered for grid independence study were refined by first varying the number of elements around the blade section, and then by varying the dimension of the elements in the circular refinement zone around the blade section. The lift coefficient (C_L) is the reference quantity for the grid independence study. In figure 2a, C_L is plotted against the number of elements around the blade section. It can be noted that, for number of blade section elements greater than 800, the coefficient converges. Hence, further increase of blade section elements would not affect the solution. Therefore, C_L was estimated as a function of increasing number of mesh elements in figure 2b. Due to convergence of the coefficient above 841865 mesh elements, grid independence was reached, and grid having 841865 elements was selected for the analysis.

3.2. Flow dynamics

The effects of the RANS turbulence models employed on the mean flow features were first assessed. RANS results of present investigation were compared with those coming from the DNS introduced in Section 2.3. First, lift (C_L) and drag (C_D) coefficients were used as global quantities to assess any discrepancies between the adopted models and DNS results. In table 1, such a comparison is reported by also considering previous experimental investigations on NACA 4412 profiles [17,18]. Notice that the present test case considers a rather atypical combination of angle of attack, Reynolds number and turbulent intensity. Hence, a direct comparison between numerical and experimental results collected in previous works could not be fully performed due to a lack of available data for same working conditions.

Table 1: Lift and drag coefficients for different numerical approaches and comparison with similar experimental cases [17,18].

Method	***Re***	***AoA***	C_L	C_D
DNS	$6.6 \cdot 10^4$	15°	1.409	0.097
Transition SST k-ω	$6.6 \cdot 10^4$	15°	1.285	0.105
Transition k-k_L-ω	$6.6 \cdot 10^4$	15°	1.534	0.115
Koca et al. [17]	$7.5 \cdot 10^4$	14°	1.3	0.15
Dwivedi et al. [18]	$1.7 \cdot 10^5$	15°	1.45	0.719

Here, it can be noticed that the Transition SST k-ω tends to underestimate the lift coefficient of DNS, while it slightly overestimates the drag coefficient. On the other hand, the Transition k-k_L-ω overestimates both lift and drag coefficients. Nonetheless, the Transition SST k-ω exhibits a slightly better agreement also with the experimental data, especially those provided in [17]. To better understand the reason behind the reported discrepancies, the pressure coefficient (Cp) and the skin friction coefficient (Cf), evaluated along the wing surfaces, were considered for comparison between the present turbulence models and the DNS results in figure 3a and figure 3b, respectively.

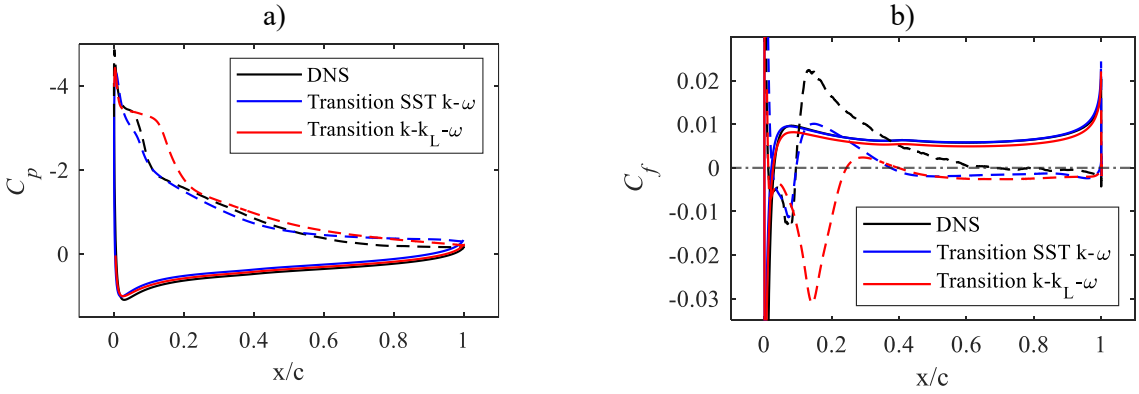

Figure 3: Comparison between RANS and DNS; pressure coefficient (a), skin friction coefficient (b). Solid line: pressure side; dashed line: suction side.

Notice that the DNS highlights, in figure 3, the formation of a LSB, which is identified by a plateau in C_p along the suction side, close to the leading edge. While both turbulence models can reconstruct the

trend provided by the DNS over the pressure side of the airfoil, both methods fail, to some extent, to reproduce the C_p along the suction side. While the Transition SST k-ω tends to follow in a more precise way the stabilization of C_p caught by the DNS at the LSB, the Transition k-k_L-ω exhibits a wider plateau, suggesting a rather heavy overestimation of LSB length. On the other hand, both models tend to slightly differ from the DNS result close to the trailing edge, where the final separation of the turbulent boundary layer occurs. The skin friction coefficient of figure 3b confirms the poor capability of the Transition k-k_L-ω of accurately reproducing the LSB length. In fact, C_f estimated by the Transition k-k_L-ω assumes negative values for a wider range of x/c than the Transition SST k-ω.

3.3. Heat transfer

Heat transfer quantities were also collected during computations. In figure 4, the local Nusselt number (*Nu*) evaluated over the wing surface is shown for the three different methodologies. Specifically, Nusselt number was locally evaluated as $Nu = -dT/d\hat{n}\ (c/(T_0-T_w))$.

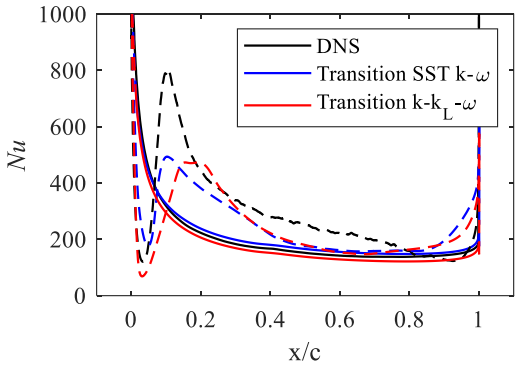

Figure 4: Comparison between RANS and DNS local Nusselt number. Solid line: pressure side; dashed line: suction side.

A very good agreement between turbulence models and DNS is perceivable at the leading edge and over the pressure side. For what concerns most of the suction side, Nu is underestimated by both turbulence models. Such a discrepancy is stronger at the LSB location probably due to a general underestimation of the recirculating flow magnitude.

4. Conclusions

A NACA 4412 profile was numerically investigated through a steady RANS approach to find the best transitional model able to reproduce the main aerodynamic and thermodynamic features under low Reynolds number and high AoA. Specifically, tests were performed at Re = 66000 (chord-based), AoA = 15° and level of the free-stream turbulence TI = 5%. Simulations were carried out through Ansys Fluent© (v. 2023 R1). Results provided by Transition SST k-ω and the Transition k-k_L-ω models were studied and compared with DNS data. The results highlighted that, for the present study case, the Transition SST k-ω model was the more accurate, not only in terms of global aerodynamic coefficients, but also in catching transitional features of the separated flows, such as length of the LSB. In fact, the latter was overestimated, by the Transition k-k_L-ω, by more than double. On the other hand, *Nu* was similarly predicted by both methods, despite the Transition SST k-ω was able to better identify the exact location of *Nu* peak at the LSB.

Acknowledgments

The Authors would like to acknowledge financial support from PNRR MUR project ECS_00000033_ECOSISTER.

References

[1] Bin Abu Sofian A D A, Lim H R, Siti Halimatul Munawaroh H, Ma Z, Chew K W and Show P L 2024 Machine learning and the renewable energy revolution: Exploring solar and wind

energy solutions for a sustainable future including innovations in energy storage *Sustainable Development* 1-26

[2] Keith D W, DeCarolis J F, Denkenberger D C, Lenschow D H, Malyshev S L, Pacala S and Rasch P J 2004 The influence of large-scale wind power on global climate *Proceedings of the National Academy of Sciences* **101** 16115–16120

[3] Tummala A, Velamati R K, Sinha D K, Indraja V and Krishna V H 2016 A review on small scale wind turbines *Renewable and Sustainable Energy Reviews* **56** 1351–1371

[4] Wang S, Zhou Y, Alam Md M and Yang H 2014 Turbulent intensity and Reynolds number effects on an airfoil at low Reynolds numbers *Physics of Fluids* **26** 115107

[5] Wauters J and Degroote J 2018 On the study of transitional low-Reynolds number flows over airfoils operating at high angles of attack and their prediction using transitional turbulence models *Progress in Aerospace Sciences* **103** 52–68

[6] Anitha D, Shamili G K, Ravi Kumar P and Sabari Vihar R 2018 Air foil shape optimization using cfd and parametrization methods *Mater. Today Proc.* **5** 5364–5373

[7] Liu J, Chen R, Lou J, Wu H, You Y and Chen Z 2023 Airfoils optimization based on deep reinforcement learning to improve the aerodynamic performance of rotors, *Aerosp. Sci. Technol.* **143** 108737

[8] Li J, M. Zhang, Tay C M J, Liu N, Cui Y, Chew S C and Khoo B C 2022 Low-Reynolds-number airfoil design optimization using deep-learning-based tailored airfoil modes *Aerosp. Sci. Technol.* **121** 107309

[9] Liu Y, Li P and Jiang K 2021 Comparative assessment of transitional turbulence models for airfoil aerodynamics in the low Reynolds number range *Journal of Wind Engineering and Industrial Aerodynamics* **217** 104726

[10] Rezaeiha A, Montazeri H and Blocken B 2019 On the accuracy of turbulence models for CFD simulations of vertical axis wind turbines *Energy* **180** 838–857

[11] Michna J, Rogowski K, Bangga G and Hansen M O L 2021 Accuracy of the gamma re-theta transition model for simulating the DU-91-W2-250 airfoil at high reynolds numbers *Energies* **14**

[12] Liu Y, Zhang Z, Tian W and Hu H 2020 An experimental investigation on the dynamic ice accretion and unsteady heat transfer over an airfoil surface with embedded initial ice roughness *Int. J. Heat. Mass. Transf.* **146** 118900

[13] Menter F R, Langtry R B, Likki S R, Suzen Y B, Huang P G and Völker S 2004 A Correlation-Based Transition Model Using Local Variables—Part I: Model Formulation, *J. Turbomach.* 413–422

[14] Kato M and Launder B E 1993 The modeling of turbulent flow around stationary and vibrating square cylinders *Ninth Symposium on "Turbulent Shear Flows* Kyoto Japan

[15] Walters D K and Leylek J H 2004 A New Model for Boundary Layer Transition Using a Single-Point RANS Approach *J. Turbomach.* **126** 193–202

[16] Fischer P F, Lottes J W and Kerkemeier S G nek5000 Web page

[17] Koca K, Genç M S, Açıkel H H, Çağdaş M and Bodur T M 2018 Identification of flow phenomena over NACA 4412 wind turbine airfoil at low Reynolds numbers and role of laminar separation bubble on flow evolution *Energy* **144** 750–764

[18] Dwivedi Y D, Wahab A, Pallay A D and Shesham A 2022 Effect of surface roughness on aerodynamic performance of the wing with NACA 4412 airfoil at Reynolds number 1.7×10^5 *Mater. Today. Proc.* **56** 468–476